J. Nonlinear Sci. Vol. 1: pp. 147–173(1991)

Journal of Nonlinear Science

Topological Analysis of Chaotic Time Series Data from the Belousov-Zhabotinskii Reaction

G. B. Mindlin[1], H. G. Solari[1,2], M. A. Natiello[3], R. Gilmore[1], and X.-J. Hou[1]

[1] Department of Physics and Atmospheric Science, Drexel University, Philadelphia, PA 19104, USA

[2] Present address: Departamento de Física, FCEN-Universidad de Buenos Aires, Pabellón I, Ciudad Universitaria, 1428 Buenos Aires, Argentina

[3] Department of Quantum Chemistry, Uppsala University, Box 518, S751, 20 Uppsala, Sweden

Received October 29, 1990; accepted for publication April 22, 1991
Communicated by Philip Holmes

Summary. We have applied topological methods to analyze chaotic time series data from the Belousov-Zhabotinskii reaction. First, the periodic orbits shadowed by the data set were identified. Next, a three-dimensional embedding without self-intersections was constructed from the data set. The topological structure of that flow was visualized by constructing a branched manifold such that every periodic orbit in the flow could be held by the branched manifold. The branched manifold, or induced template, was computed using the three lowest-period orbits. The organization of the higher-period orbits predicted by this induced template was compared with the organization of the orbits reconstructed from the data set with excellent results. The consequences of the presence of certain knots found in the data are discussed.

Key words. strange attractor, template, time series data

1. Introduction

It has recently become possible to classify strange attractors by integers [1]. This makes possible the identification of chaotic time series data in terms of the integer invariants which classify the strange attractor in which the motion takes place. It is the purpose of the present work to illustrate how this procedure may be carried out

on experimental time series data. The data which are classified have been generated by the Texas group and described by Coffman et al. [2] and Richetti et al. [3].

At present, there are two distinct approaches to the analysis of chaotic time series from low-dimensional strange attractors. These are the metric [4,5,6] and the topological approaches [1,7,8,9].

The metric approach is based on distances. Distances between points in appropriate embeddings of the data are used to compute a set of metric properties. These include fractal (or other) dimension [4], Lyapunov exponent [5], and the spectrum of singularities, $f(\alpha)$ [10]. These quantities are averaged over the strange attractor. They are difficult to compute [11], require large data sets, and degrade rapidly with additive noise. The results of such computations are real numbers with error bars which are difficult to verify independently and, having been designed with different aims, are not extremely useful in providing insights on "how to model the dynamics" [8].

The topological approach is based on organization. Embedded within a hyperbolic strange attractor is a dense set of unstable periodic orbits [12]. In the case of three-dimensional flows, the periodic orbits are closed curves that can be characterized by the way in which they are knotted and linked with each other. Moreover, if a Poincaré section exists for the flow, any finite set of periodic orbits can be identified with an element in the Braid group (up to conjugation). What allows a systematic study of these features is that, in the case of hyperbolic flows, there is a one to one correspondence between the periodic orbits in it and the orbits carried by a branched manifold [13]. Moreover, the orbits in the real flow and the ones in the "knot holder" or template share the same topological properties. If the template that carries the periodic orbits is identified, the organization of the orbits is known even when parameters are changed and hyperbolicity is lost, as an orbit cannot change its knot type or linking numbers as parameters are changed.

We say that a three-dimensional flow is compatible with an *induced* template when all the periodic orbits of the flow can be associated with periodic orbits of the induced template in such a way that the braid structure is preserved. This association is weaker than the one obtained through the Birman-Williams-Holmes procedure for hyperbolic sets, where there is a one to one correspondence between orbits in a flow and orbits in the template [13,14,15,16,17]. In practical terms, this weaker definition allows us to expect all the periodic orbits in a non-hyperbolic flow to be represented by orbits in the knot holder, in contrast with the original approach which would force us to restrict attention to subsets of the phase space having the appropriate hyperbolic structure; the price paid for this advantage is to have orbits in the knot holder without a counterpart in the flow. Consequently, flows differing in the spectra of orbits but sharing the same organization might not be distinguished in this classification. Our induced template provides us with a model for the qualitative dynamics of the flow.

In this paper we analyze chaotic time series data from the Belousov-Zhabotinskii reaction. This chemical reaction has been modeled by a high-dimensional ($n > 3$) dynamical system [18]. It is therefore not obvious that the Birman-Williams theorem, valid for flows with one unstable direction in three manifolds, is even applicable. We find, however, that we can construct an embedding of the scalar time series data (logarithm of the bromine ion concentration) in $\mathbb{R}^3$ and construct an induced tem-

plate which is compatible with the flow. The flow itself is probably not hyperbolic. The point is that the topological properties (knot type, linking numbers) of the orbits which exist in the hyperbolic limit are properties of the knots themselves, and not of the induced template, which provides a convenient mechanism for computing these properties. Thus, they remain invariant for those knots which are embedded in the invariant set, even if it is not hyperbolic.

The induced template serves two functions. First, it provides a qualitative model for the dynamics generating the observed time series data. Second, it can be used to screen models which attempt to describe these data. If time series generated by a model and an experiment, embedded in the same way in a three-dimensional manifold, induce the same template, the model is not incompatible with the data. If different templates are induced, the model cannot provide a valid description of the processes generating the experimental time series.

The paper is organized as follows. The steps required to implement the topological analysis of chaotic time series data are reviewed in Sec. 2. These are then carried out in the subsequent sections. In Sec. 3 we illustrate how to extract information about unstable periodic orbits from the chaotic time series data using the method of close returns. In Sec. 4 we discuss the strengths and weaknesses of various embedding procedures. In Sec. 5 we construct a branched manifold compatible with the data from the low-period orbits reconstructed in Sec. 3 and the embedding of Sec. 4. In Sec. 6 we illustrate how the template identification is validated using the higher-period orbits reconstructed in Sec. 3. In Sec. 7 we discuss the qualitative dynamics which generate the Belousov-Zhabotinskii data in terms of the induced template. The methods presented in this work raise a large number of questions. These are presented and discussed in Sec. 8. We conclude with a summary of this method and results in Sec. 9.

2. Outline of Procedure

The topological approach is based on the organization of unstable periodic orbits embedded in the strange attractor [1,7,8,9]. The first step is therefore the extraction of periodic orbits from the chaotic time series data. This is accomplished by a search for close returns in the data. The procedure for extracting these orbits is described in Sec. 3.

We will construct a three-dimensional flow from the data, even though the data may be generated by a high-dimensional ($n > 3$) dynamical system. This requires a three-dimensional embedding of the scalar data experimentally recorded. For our purposes, a good embedding will necessarily be one in which there are no self-intersections of the flow. We explore alternative embedding methods in Sec. 4. We adopt an embedding involving a differential and an integral filter. In what follows we restrict our attention to fully expanding templates, that is, those templates associated with full shifts, as in reference [1] (see Figure 1).

A template can be constructed from the period 1 and period 2 orbits. When some of these are not present in the data set studied, one has to resort to higher-period orbits.

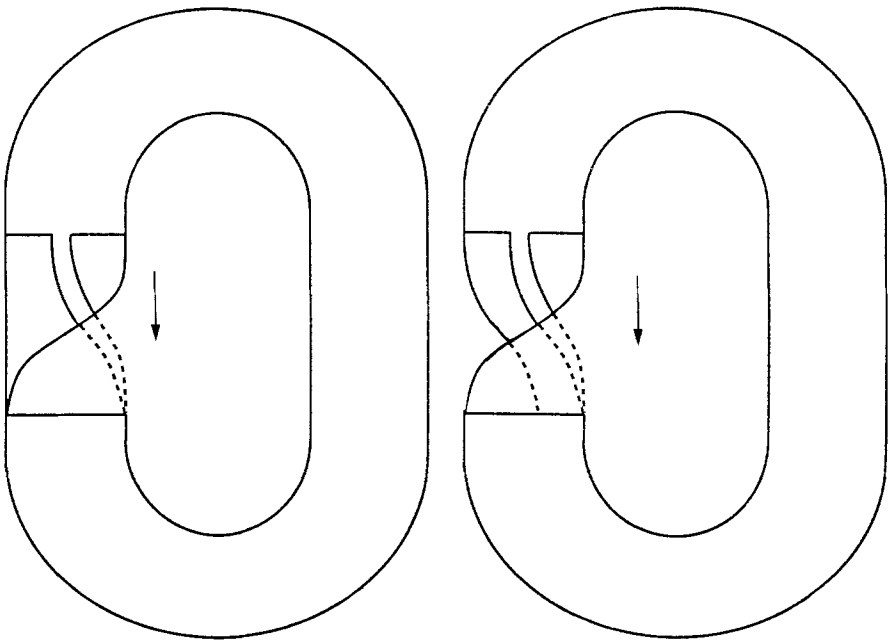

Fig. 1. Two different templates are shown in this figure. In both cases, the periodic orbits that can be supported by them can be characterized by finite sequences of two symbols that indicate which branches (left or right) are visited, and in which order. For the template on the left, an arbitrary sequence of two symbols is the name of a periodic orbit. We call these templates fully expansive. For the template on the right, after visiting the left branch we visit the right one. Therefore, not every sequence of two symbols represents an orbit in this template. We call these templates not fully expansive.

A template is classified by a square $n \times n$ matrix and an $n \times 1$ array, where n is the number of branches (components) in the branched manifold [1]. This is also the number of distinct period-one orbits embedded in the hyperbolic strange invariant set. The $n \times n$ matrix is symmetric and integer valued. The ith diagonal element is the local torsion around the ith period-one orbit. This is the angle through which the flow twists in one period in the neighborhood of the period 1 orbit, measured in units of π. The (i, j)th matrix element is twice the linking number of the ith and jth period-one orbits. The linking number of two periodic orbits is the signed number of times either passes through a surface bounded by the other. Diagonal elements of this matrix are integers, even or odd depending on whether the orbit is an orientation-preserving (regular) or orientation-reversing (flip) saddle. All off-diagonal elements are even. The order in which the n branches of the branched manifold are identified at the branch line is determined by the $n \times 1$ array. This information is extracted from the organization of the $\binom{n}{2}$ period 2 orbits with respect to the period 1 orbits.

Once the induced template has been identified, it can be used to predict the topological properties of all remaining orbits embedded in the strange attractor. These

properties include the following:

1. The linking numbers of all pairs of periodic orbits [19].
2. The relative rotation rates of all pairs of periodic orbits [20].
3. The self-linking number of each periodic orbit.
4. The relative rotation rates for each periodic orbit.
5. The local torsion around each periodic orbit [19,20].
6. The knot polynomials (Conway, Jones, Alexander, ...) for each periodic orbit [21].

These predictions are fixed by the induced template matrix and array. The properties of orbits remain unchanged while the orbits exist, even when control parameters or experimental conditions are changed so that the invariant set is no longer hyperbolic.

On the other hand, these properties can also be computed directly from the periodic orbits reconstructed from the time series data. Comparison of the predictions with the directly measured values can be used to invalidate or increase confidence in the template identification. This procedure is carried out in Sec. 6.

The flow over the branched manifold provides a qualitative description of the mechanism responsible for generating the original time series data [16]. In general, only a subset of all periodic orbits in the induced template exists in this flow. A systematic study of which periodic orbits are embedded in a chaotic attractor is not a solved problem. There are, however, some partial results. One of these is that the presence of "badly ordered" orbits [22] implies that the topological entropy of the flow is greater than zero. We have extracted one of these orbits (of period seven, knotted as a $(7,3,-2)$ pretzel). As a result, it is unnecessary to resort to dimension or entropy calculations to show that the data set is chaotic.

3. Search for Close Returns

Periodic orbits have previously been extracted from this data set [23]. The extraction procedure used depended on a three-dimensional delay embedding.

The reconstruction of periodic orbits is independent of embedding and can be carried out by searching for close returns directly in the original time series data $x(i), i = 1, 2, \ldots, N$. One very colorful method involves color coding the difference

$$|x(i) - x(j)| \tag{1}$$

and plotting (1) as a function of the indices i and j. The difference vanishes along the diagonal $i = j$. Close returns reveal themselves as segments parallel to and offset from the diagonal.

A better procedure involves color coding the difference

$$|x(i) - x(i + p)| \tag{2}$$

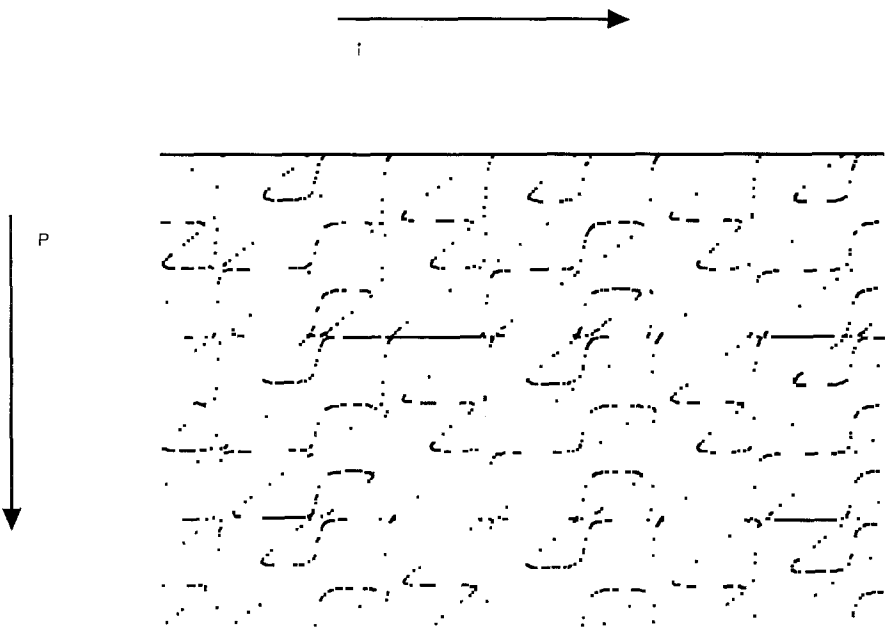

Fig. 2. Close returns plot for part of the Belousov-Zhabotinskii data. The point (i, p) is colored black if the distance $(|x(i) - x(i+p)|)$ is less than some (ϵ), typically about 1% of the maximal distance $(MAX|x(i) - x(j)|)$. Nearly horizontal line segments reveal part of the time series in the neighborhood of an unstable periodic orbit. The Belousov-Zhabotinskii data set has length 64 K. The portion shown in this plot has range $1 \leq i \leq 1000$ and $0 \leq p \leq 960$. One of the data segments near the unstable period 3 orbit (011) appears as a horizontal line segment from $i = 240$ to $i = 430$ with $p = 370$. Other orbits used to construct and verify the induced template are observed in other close returns plots (different ranges of i).

and plotting (2) as a function of i (horizontal) and p (vertical). Such a plot is shown in Figure 2 for a segment of the Belousov-Zhabotinskii time series. In such a plot, periodic data will generate a series of equally spaced horizontal lines, stochastic data will generate a random pattern, and chaotic data will generate a series of almost horizontal line segments. Adding noise to the chaotic data sets will simply decrease the resolution of the lines representing close returns. The vertical offset indicates the period, p (measured in units of the sampling time), of the periodic orbit which the chaotic time series data are shadowing. The beginning and endpoints, i_i, i_f, indicate the location in the data set (i_i to $i_f + p$) of the segment which closely follows this periodic orbit. This segment can be extracted and used either directly as a representation of this periodic orbit or else combined with other similar segments to construct a weighted average of this unstable periodic orbit.

Many unstable periodic orbits have been extracted from the Belousov-Zhabotinskii data using this procedure. These orbits, and some of their properties, are listed in Table 1.

Table 1. Periodic orbits reconstructed from chaotic time series data from the Belousov-Zhabotinskii reaction.

Orbit	Period	Symbolics	Local Torsion	Self-Linking
1	1	(1)	1	0
2	2	(01)	1	1
3	3	(011)	2	2
4	4	(0111)	3	5
5	5	(01011)	3	8
6	6	(0110*M*1)*	3	9
7	7	(0101011)	4	16
8*a*	8	(01011011)	5	21
8*b*	8	(01010111)	5	23
9	9	$(01)^3(011)$	5	28
10*a*	10	$(01)^2(011)^2$	6	33
10*b*	10	$0111(011)^2$	7	33
11	11	$(01)(011)^3$	7	40
13*a*	13	$(01)^2011010111$	8	62
13*b*	13	$(01)^30110111$	8	60
13*c*	13	$(011)^30101$	8	56
13*d*	13	$(011)^30111$	9	56
13*e*	13	$(01)^2011011111$	9	62
14	14	$(01)(011)^4$	9	65
15	15	$(01)(011)^20111011$	10	78
16*a*	16	$(01)^3(011)^20111$	10	89
16*b*	16	$(011)^40101$	10	85
16*c*	16	$(011)^40111$	11	85
16*d*	16	$(01)^2(011)^2011111$	11	91
17*a*	17	$(01)^301101(011)^2$	10	102
17*b*	17	$(01)(011)^5$	11	96
17*c*	17	$(01)^201101(0111)^2$	11	108

* M transits the cut separating the orientation-preserving and orientation-reversing components of the template.

We emphasize again that the reconstruction of periodic orbits does not require any embedding[1] and can be carried out directly on scalar time series data. Further, lack of close returns is a strong indication that the data are not generated by motion on a low-dimensional strange attractor. Sensitivity of the search for close returns to additive noise is discussed in Sec. 8.

[1] We assume, as usual, that a sufficiently long segment of the time series contains enough information to determine the dynamics. In symbols, we assume that there is a sufficiently large integer n_0 such that if the time series $X = (\ldots, x_i, x_{i+1}, \ldots, x_{i+n}, \ldots)$ and $Y = (\ldots, y_i, y_{i+1}, \ldots, y_{i+n}, \ldots)$ have an identical segment of length $n \geq n_0$, then $X = Y$; which is to say that the time series can always be represented in an n-dimensional time-delay embedding for some sufficiently large n.

4. Embedding

Although periodic orbits can be extracted from data without an embedding, the topological properties in which we are interested (cf. Sec. 2, 1–6) cannot be described unless a three-dimensional embedding can be found.

Embeddings have been described in the mathematics literature. Whitney [24] has shown that an n-dimensional manifold M^n can be embedded in $\mathbb{R}^k$ if $k \geq 2n$. If $k \geq 2n + 1$, the embedding can be made analytic. Takens has shown that when the motion occurs in M^n, the time-delay coordinates $x(i) \to \mathbf{y}(i)$,

$$\mathbf{y}(i) = \big(x(i), x(i + \tau), \ldots, x(i + 2n\tau)\big), \tag{3}$$

can be used as an embedding of M^n into $\mathbb{R}^{2n+1}$ [25]. He has even suggested that there is an embedding in terms of successive derivatives of $\mathbf{y}$ in which the dynamical system assumes the canonical form

$$\begin{aligned} \frac{dy_1}{dt} &= y_2, \\ \frac{dy_2}{dt} &= y_3, \\ &\vdots \\ \frac{dy_{2n}}{dt} &= y_{2n+1}, \\ \frac{dy_{2n+1}}{dt} &= f(y_1, y_2, \ldots, y_{2n}, y_{2n+1}). \end{aligned} \tag{4}$$

We made a number of attempts to construct a three-dimensional embedding of the Belousov-Zhabotinskii data looking especially for embeddings of the form of Eq. 4.

The reason for our preference for embeddings of the form (4), which we call differential phase space embeddings, is as follows: First, they reflect a dynamics which can generate the time series data. Second, the topological organization can be seen by inspection. For example, if two orbits cross in a phase space plot as shown in Figure 3, then since the slope at the crossing point is

$$\frac{dv}{dx} = \frac{dv/dt}{dx/dt} = \frac{x''}{x'} \tag{5}$$

with

$$v = x', \tag{6}$$

it is a simple matter to determine which orbit crosses over which by inspection. Third, if such an embedding exists, the attractor always has a "hole" in the middle (cf. Sec. 8). This guarantees the existence of a cross section and the possibility of constructing a first return map.

The $x - x'$ projection of a phase space embedding of the Belousov-Zhabotinskii data in terms of the variables x, x', and x'' is shown in Figure 4. Since all crossings

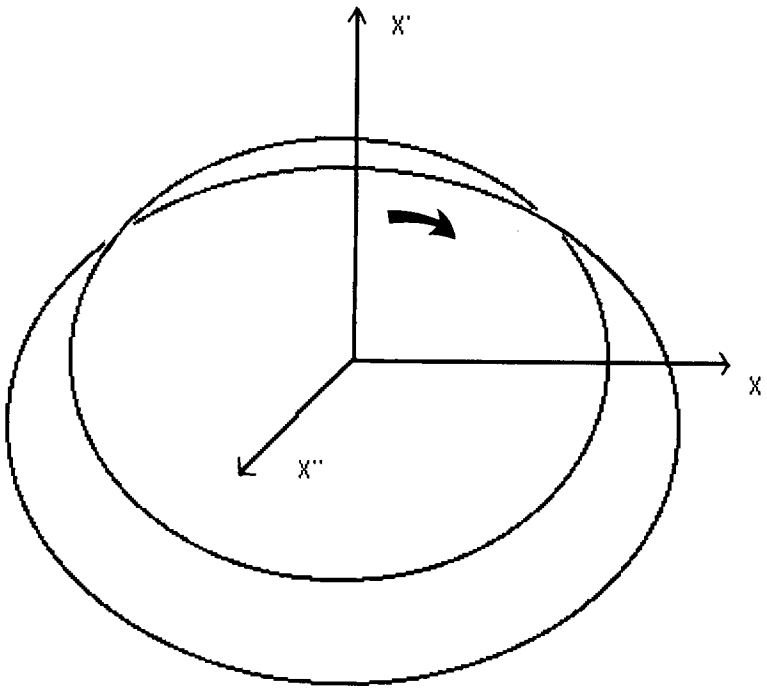

Fig. 3. When two orbits cross in the $(x' - x)$ projection of a differential phase space plot, information about which orbit crosses over (under) the other is easily determined by inspection. (cf., Eq. (7)). The flow is clockwise in this projection.

occur in the thin section, which could not be further resolved, the topological organization of the strange attractor could not be resolved in this embedding. We therefore considered a larger class of embeddings.

All the embeddings which we considered consisted of time-delay coordinates for different delays, τ, as well as a variety of differential and integral filters. The different embeddings were compared using the minimum redundancy criteria introduced by Fraser [26]. Using these criteria, the best embedding resulted from the use of two integral filters and the measured variable itself

$$y_1(i) = x(i), \quad y_2 = \sum_{j=1}^{i} x(i)e^{(j-i)/\beta_1}, \quad y_3(i) = \sum_{j=1}^{i} x(i)e^{(j-i)/\beta_2}. \tag{7}$$

This class of embeddings exhibited self-intersecting attractors violating the necessary condition stated in Sec. 2. The self-intersection was simple to recognize beyond any possible doubt in three-dimensional plots, $(x, y, color)$, of the attractor. Such a possibility was already considered in [26].

The second-best embedding, according to Fraser's test, consisted of the variable itself, an exponential filter and the first difference of the variable. These variables can

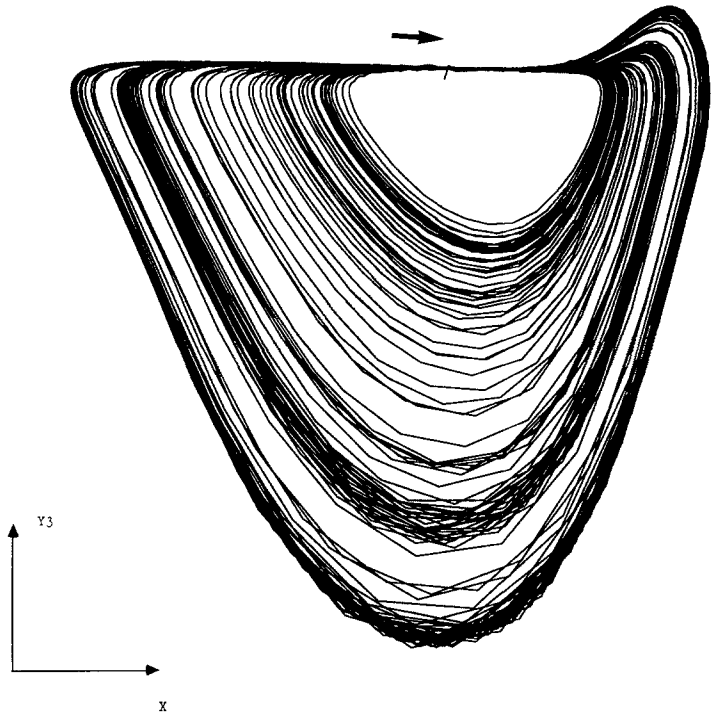

Fig. 4. Phase space embeddings x' vs. x for data from the Belousov-Zhabotinskii reaction. Interpretation of the topological organization of the strange attractor is difficult because all crossings occur in the thin section. The flow is clockwise around the hole.

be considered as representative of a flow of the form

$$\begin{aligned} \frac{dy_1}{dt} &= -(1/\tau)y_1 + x, \\ y_2 &= x, \\ y_3 &= x', \end{aligned} \tag{8}$$

where

$$\begin{aligned} y_1(i) &= \sum_{j=1}^{i} (x(j)e^{-(i-j)/\tau}), \\ y_2(i) &= x(i), \\ y_3(i) &= x(i) - x(i-1). \end{aligned} \tag{9}$$

This was the embedding finally adopted. The projection of the embedded Belousov-Zhabotinskii data onto the $y_1 - y_2$ plane is shown in Figure 5. In this projection all

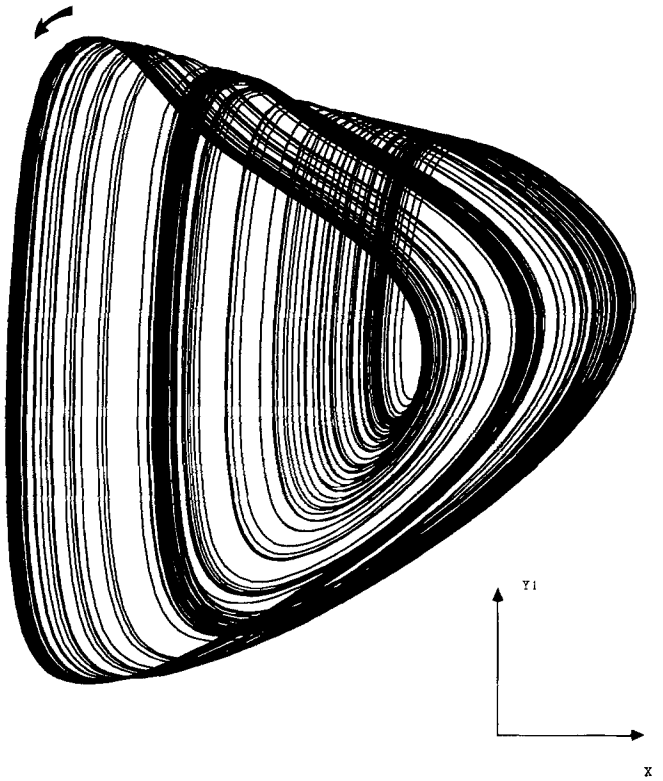

Fig. 5. Embeddings of the data for the Belousov-Zhabotinskii reaction determined from the filter defined by Eq. (8). The flow is counterclockwise around the hole in the middle.

over- and under-crossings are clearly resolved. Projection onto the $y_2 - y_3$ or $x - x'$ plane has previously been shown in Figure 4.

We emphasize that the process of filtering was introduced to generate a new variable rather than to eliminate noise. A discussion related to the effects of noise reduction and data filtering on the metric characterization of attractors can be found in [27].

With respect to other possible embeddings considered, we can say that, in general, they presented resolution problems when trying to evaluate the braid structure of the periodic orbits. Differential embeddings decrease the signal to noise ratio making it impossible for us to resolve the under- and over-crossings. Time-delay embeddings of the form (3), optimized by changing τ, also presented regions of the flow where it was not possible to resolve the braid structure.

The embedding adopted, Eq. (8), allows us to find a Poincaré section. Two "Poincaré cuts" are shown in Figure 6, as well as the return maps $\big(x(i+1)$ vs $x(i)\big)$ on these Poincaré sections. The existence of a good one-dimensional return map allows the development of a symbolic dynamics: 0 for the orientation-preserving branch and 1 for the orientation-reversing branch. The symbolic dynamics for each of the reconstructed orbits is shown in Table 1.

Although the existence of a reasonably good one-dimensional map associated with the flow facilitates the assignment of symbolic names to the periodic orbits, such a

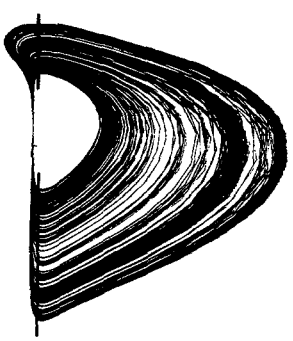

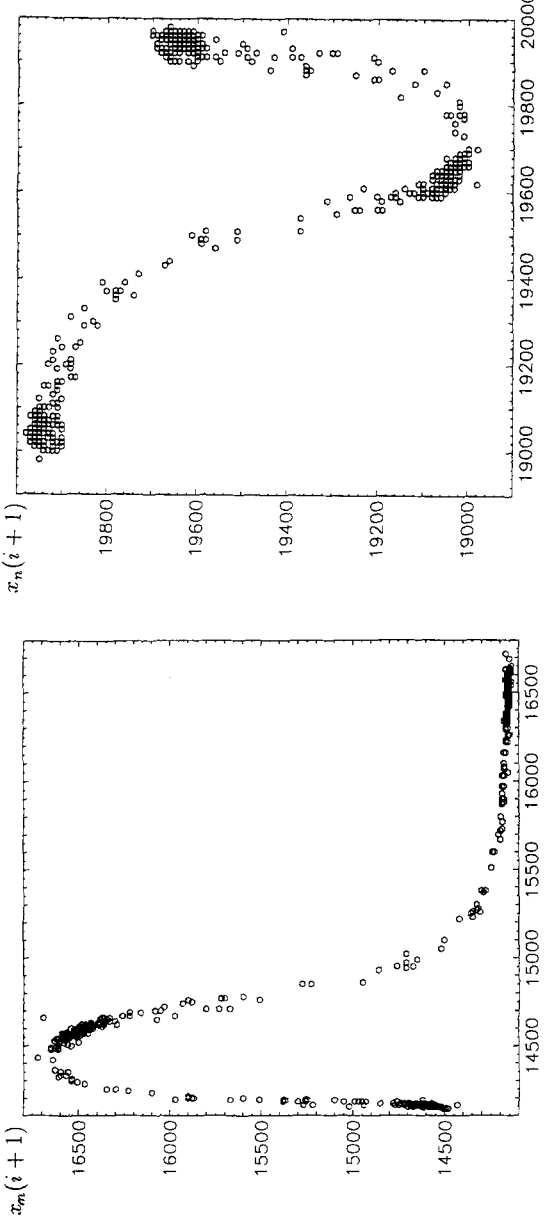

Fig. 6. Return map $x(i+1)$ vs. $x(i)$ on the cuts $x' = 0$ of the Belousov-Zhabotinskii strange attractor. (a) Return map on the plane $x' = 0, x'' < 0$ and (b) return map on the plane $x' = 0, x'' > 0$. Inset: cuts in the strange attractor on which the return maps are constructed.

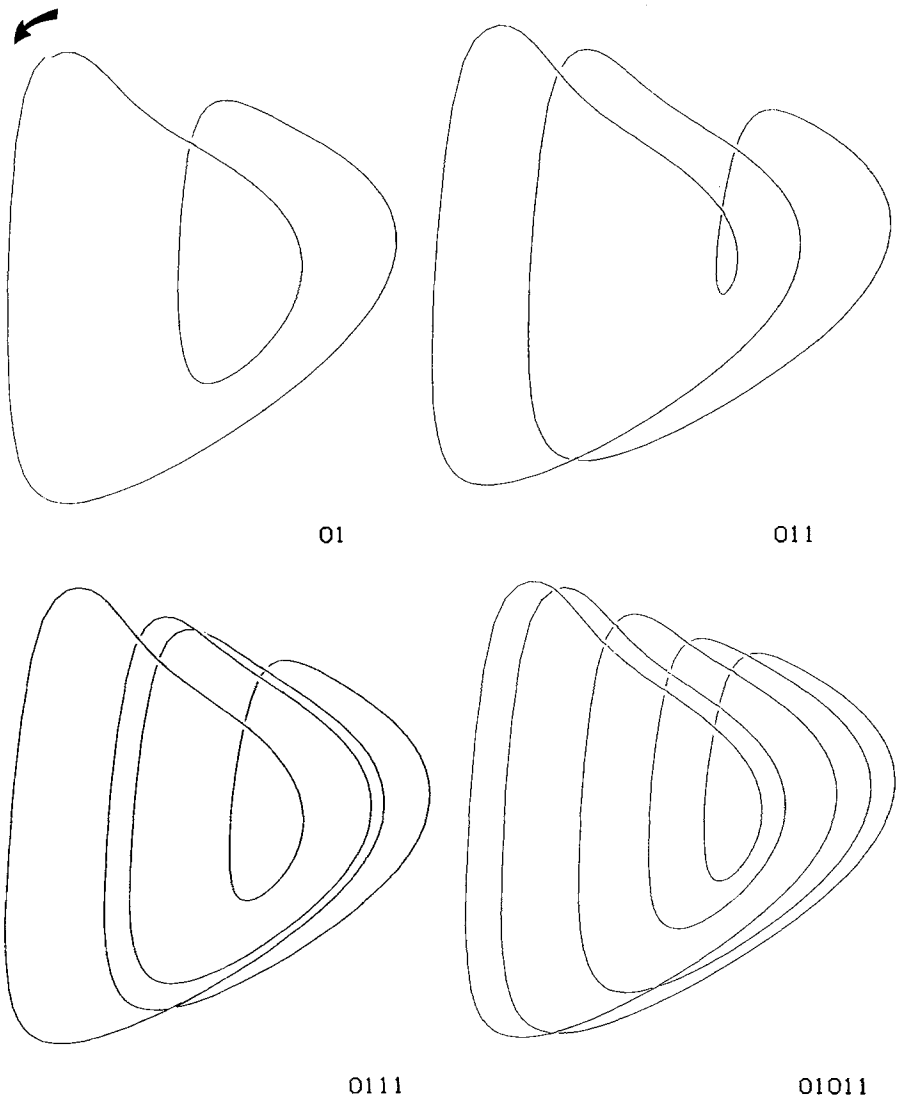

Fig. 7. Orbits of period 2, 3, 4, and 5 reconstructed from time series data from the Belousov-Zhabotinskii reaction and projected onto the y_1, y_2 plane of the embedding given in Eq. (9). The over- and under-crossings are clearly shown. The flow is counterclockwise.

map is not necessary. Symbolic names are given to the periodic orbits such that they have the same name as the associated orbits in the induced template, once the template has been determined. Both procedures give consistent results in the present study.

Once the embedding has been established, the topological properties of the periodic orbits reconstructed from the data are determined. These segments have been extracted from the data using the method of close returns discussed in Sec. 3. A number of periodic orbits are shown in Figure 7 projected onto the (y_1, y_2) plane of the embedding

defined by Eq. (9). Each is identified by its symbolic dynamics, and the over- and under-crossings are shown for each. Since all orbits are plotted to the same scale, linking properties of a pair can be determined by superposing the two orbits and counting the signed number of crossings (cf. Sec. 6).

5. Construction of the Induced Template

The general procedure for constructing templates, summarized earlier, will now be described in more detail and applied in the case of the Belousov-Zhabotinskii strange attractor. First, the complete set of period 1 orbits is constructed. All segments representing the ith period-1 orbit are compared pairwise. The signed number of times each pair crosses is typically invariant over all pairs representing the same orbit. This integer, $l(i)$, is the local torsion of the ith period 1 orbit.

Then the linking number of each segment representing the ith period 1 orbit is computed with each segment representing the jth period 1 orbit. These integers should also be invariant over all periodic pairs. This integer, $l(i, j)$, is the linking number of the ith and jth period 1 orbit.

In computing the integers $l(i)$ and $l(i, j)$, we adopt the following sign convention. At each crossing point tangent vectors t_1 and t_2 are drawn to the upper and lower curve segments in the direction of the flow. The crossing is labeled $+1$ (-1) if the tangent vectors form a right- (left-) handed coordinate system in the projection plane (see Figure 3).

The template matrix has diagonal matrix elements $l(i)$ and off-diagonal matrix elements $2l(i, j) = 2l(j, i)$.

The order in which the n-branches of the template are joined on the branched line is determined by the n-element array. By convention, the higher the integer, the nearer the front the component occurs in compression. This information is determined by computing the linking number of the period 2 orbits with the period 1 orbits. This in fact overdetermines the $n \times 1$ array if $n > 2$.

Construction of the template is not quite so straightforward for the Belousov-Zhabotinskii attractor. The return map strongly suggests that the template has two branches. Its algebraic description is therefore

$$\begin{pmatrix} l(0) & 2l(0,1) \\ 2l(1,0) & l(1) \end{pmatrix}, \qquad (10)$$
$$(0 \quad m),$$

where $m = \pm 1$. As can be inferred by inspection of the return map, no segments resemble the period 1 orbit (0) through the orientation-preserving branch of the template. Two segments in the data set resemble the period 1 orbit (1) in the orientation-reversing component of the template. The local torsion computed using this pair of segments is $l(1) = 1$.

A periodic orbit (01011 . . .) which passes p_0 (p_1) times through the orientation-preserving (-reversing) branch has local torsion $p_0 l(0) + p_1 l(1)$. Since the local torsion of the period 2 orbit (01) is 1, $l(0) = 0$.

The linking number $l(0, 1)$ and order information m are determined by computing how the period 1 orbit (1) links the period 2 (01) and period 3 (011) orbits. The results are

$$\begin{aligned} L\big((1), (01)\big) &= l(0, 1) + \frac{1}{2}(m + 1) = 1, \\ L\big((1), (011)\big) &= l(0, 1) + 1 = 1, \\ L\big((01), (011)\big) &= 3l(0, 1) + (m + 1) = 2. \end{aligned} \tag{11}$$

The integers on the right were computed by superposing the orbits (1) and (01), (1) and (011), and also (01) and (011). The result is $l(0, 1) = 0, m = 1$ and the following classification of the template by integers

$$\begin{pmatrix} 0 & 0 \\ 0 & 1 \end{pmatrix}, \qquad (0 \quad 1). \tag{12}$$

This set of integers characterizes a flow with Smale horseshoe return map and zero global torsion in suspension [1, 14, 17] (see Figure 1).

6. Template Verification

The topological organization of all periodic orbits and all pairs of periodic orbits is uniquely determined once the underlying template has been characterized. These properties include the following:

1. Self-linking number of single orbits.
2. Linking numbers of orbit pairs.
3. Local torsion.
4. Self-relative rotation rate.
5. Relative rotation rate of orbit pairs.
6. Knot and link polynomial invariants.

The local torsion of the orbit (01011...) (p_0 0's and p_1 1's) is $0p_0 + 1p_1$. The self-linking number is the signed number of crossings of that orbit with itself. The self-linking number of the orbits (011) and (0111) are computed in Figure 8. The local torsion and self-linking numbers computed from the template matrix are listed for each periodic orbit in Table 1.

The linking number for any pair of periodic orbits is computed similarly. The two orbits are superposed. The linking number is half the algebraic sum of signed crossings. This computation is illustrated in Figure 9 for (01) and (011). This number can also be computed algorithmically. Inputs for the algorithm include the template information (matrix and order information) and the symbolic dynamics for each orbit of

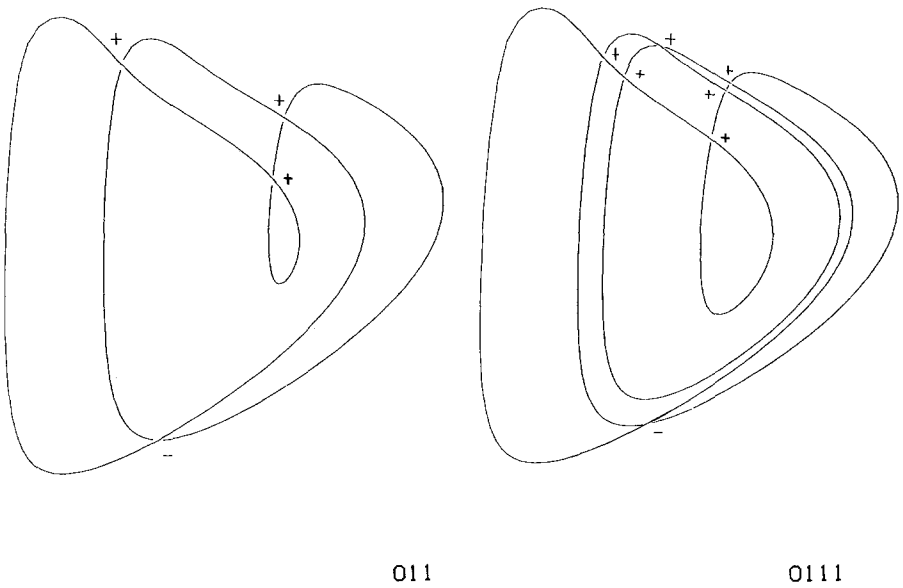

Fig. 8. Self-linking numbers of the periodic orbits are the number of signed crossings. Self-linking number for (a) orbit (011) is 2 and (b) orbit (0111) is 5. The flow is counterclockwise.

interest. The matrix of linking and self-linking numbers computed using this algorithm is presented in Table 2.

These computations were carried out for all pairs of periodic orbits up to period 8. For all but one of the periodic pairs tested the measurements (counting number of signed crossings) and predictions agreed. The discrepancy occurred between the period 4 orbit (0111) and one of the two period 7 orbit segments used to model the period 7 orbit (0101011). One period 7 orbit linked the period 4 orbit 11 times, the other 10 times. Both period 7 segments had the same symbolic dynamics. The discrepancy was traced to a lack of precision in the location of one section of a segment of data shadowing a period 7 orbit. This allowed us to prefer one period 7 orbit segment over the other.

The relative rotation rates for two periodic orbits are computed as follows. A Poincaré section is chosen and the p intersections $a_1, \ldots, a_p$ of a period p orbit and the q intersections $b_1, \ldots, b_q$ of a period q orbit are located. A difference vector $a_i - b_j$ is propagated forward pq periods, after which it returns to its original orientation by rotating through an integer multiple $\left(p * q * R_{ij}(a, b)\right)$ of 2π radians. The relative rotation rate of the difference vector $a_i - b_j$, $R_{ij}(a, b)$, is the average number of rotations, per period, made by this difference vector under forward time evolution. The relative rotation rates $R_{ij}(a, b)$ for different intersection pairs (a_i, b_j) on the Poincaré section need not all be equal [20]. The sum of the relative rotation rates over all pairs of initial conditions is the linking number of the two periodic orbits: $L(a, b) = \sum_{i,j} R_{ij}(a, b)$. The relative rotation rates of an orbit with itself are computed similarly, with the exception that $R_{ii}(a, a)$ is defined to be zero. With this convention, the sum of the self-relative rotation rates is its self-linking number.

(a)

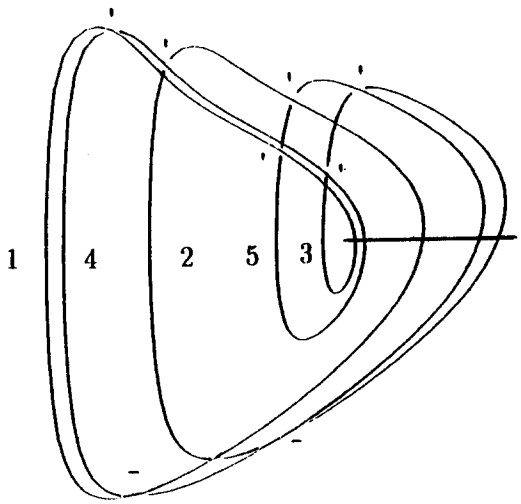

(b)

$$P(011) = \begin{bmatrix} 0 & 1 & 0 \\ 0 & 0 & 1 \\ 1 & 0 & 0 \end{bmatrix}, \quad P(01) = \begin{bmatrix} 0 & 1 \\ 1 & 0 \end{bmatrix}, \quad P = \begin{bmatrix} 0 & 1 & 0 & 0 & 0 \\ 0 & 0 & 1 & 0 & 0 \\ 1 & 0 & 0 & 0 & 0 \\ 0 & 0 & 0 & 0 & 1 \\ 0 & 0 & 0 & 1 & 0 \end{bmatrix}$$

(c)

$$C(011) = \left[\begin{array}{cc|c} 0 & 0 & 1 \\ 0 & 0 & 1 \\ \hline 1 & 1 & 0 \end{array}\right], \quad C(01) = \begin{bmatrix} 0 & 1 \\ 1 & 0 \end{bmatrix}, \quad C = \left[\begin{array}{ccc|cc} 0 & 0 & 1 & 0 & 1 \\ 0 & 0 & 1 & 0 & 1 \\ 1 & 1 & 0 & 1 & 1 \\ \hline 0 & 0 & 1 & 0 & 1 \\ 1 & 1 & 1 & 1 & 0 \end{array}\right]$$

(d)

$$2 * (n1 * n2) * RRR = \left[\begin{array}{ccc|cc} 0 & 2 & 2 & 2 & 2 \\ 2 & 0 & 2 & 2 & 2 \\ 2 & 2 & 0 & 2 & 2 \\ \hline 2 & 2 & 2 & 0 & 3 \\ 2 & 2 & 2 & 3 & 0 \end{array}\right]$$

Fig. 9. (a) The linking number of the period 2 and period 3 orbit is $\frac{1}{2}(6-2) = 2$.
(b) Permutation matrices for the individual orbits, (011) and (01), and the two orbits together.
(c) Crossing matrices for the individual orbits, (011) and (01), and the two orbits together.
(d) Matrix of relative rotation rates for the orbits, (011) and (01), computed from Eq. (13).

Table 2. Linking numbers of reconstructed periodic orbits. The period 6 orbit passes through the cut point separating the orientation-preserving from the orientation-reversing template component.

	1 1	2 01	3 011	4 0111	5 01011	6 0110*M*1	7 0101011	8*a* 01011011	8*b* 01010111
1	0								
2	1	1							
3	1	2	2						
4	2	3	4	5					
5	2	4	5	8	8				
6	2	4	6	8	10	9			
7	3	5	7	11	13	14	16		
8*a*	3	6	8	12	15	16	21	21	
8*b*	4	6	8	13	16	16	21	24	23

These rational fractions depend on initial conditions and provide phase information lacking in linking numbers. They are therefore more closely linked to physical processes than linking numbers. They have beautiful properties which provide some selection rules on the order in which bifurcations can occur in dynamical systems [20].

The relative rotation rates for orbits generated by a horseshoe have been tabulated [20]. These fractions can be computed by an algorithm whose inputs are identical to those for linking number algorithms. Relative rotation rates for the orbits extracted from the Belousov-Zhabotinskii data, up to period 8, are given in Table 3.

Table 3. Relative rotation rates of reconstructed periodic orbits

	1 1	2 01	3 011	4 0111	5 01011	6 0110*M*1	7 0101011	8*a* 01011011	8*b* 01010111
1	0								
2	$\frac{1}{2}$	$\frac{1}{2}$,0							
3	$\frac{1}{3}$	$\frac{1}{3}$	$(\frac{1}{3})^2$,0						
4	$\frac{1}{2}$	$\frac{1}{2}$,$\frac{1}{4}$	$\frac{1}{3}$	$(\frac{1}{2})^2$,$\frac{1}{4}$,0					
5	$\frac{2}{5}$	$\frac{2}{5}$	$\frac{1}{3}$	$\frac{2}{5}$	$(\frac{2}{5})^4$,0				
6	$\frac{1}{3}$	$\frac{1}{3}$	$\frac{1}{3}$	$\frac{1}{3}$	$\frac{1}{3}$	$(\frac{1}{3})^4$,$\frac{1}{6}$,0			
7	$\frac{3}{7}$	$\frac{5}{14}$	$\frac{1}{3}$	$\frac{11}{28}$	$\frac{13}{35}$	$\frac{1}{3}$	$(\frac{3}{7})^4$,$(\frac{2}{7})^2$,0		
8*a*	$\frac{3}{8}$	$\frac{3}{8}$	$\frac{1}{3}$	$\frac{3}{8}$	$\frac{3}{8}$	$\frac{1}{3}$	$\frac{3}{8}$	$(\frac{3}{8})^7$,0	
8*b*	$\frac{1}{2}$	$\frac{1}{2}$,$\frac{1}{4}$	$\frac{1}{3}$	$(\frac{1}{2})^2$,$\frac{3}{8}$,$\frac{1}{4}$	$\frac{2}{5}$	$\frac{1}{3}$	$\frac{3}{8}$	$\frac{3}{8}$	$(\frac{1}{2})^4$,$\frac{3}{8}$,$(\frac{1}{4})^2$,0

The relative rotation rates for the periodic orbits extracted from the Belousov-Zhabotinskii data can be computed as follows. Initial conditions in a Poincaré section are chosen. Then the signed number of crossings of these initial conditions is counted during each successive period, until the system returns to the initial conditions. The algebraic number of crossings is then divided by the number of periods required to return to the initial conditions.

The counting procedure is facilitated by a simple algorithm, illustrated in Figure 9. The orbit segments for the first orbit of period p_1 are numbered $1, 2, \ldots, p_1$, and those for the second orbit of period p_2 are numbered $p_1 + 1, p_1 + 2, \ldots, p_1 + p_2$. This is shown in Figure 9 for the period 3 orbit (011) and period 2 orbit (01) extracted from the Belousov-Zhabotinskii data. The segments are defined with respect to the cross section shown in Figure 9a. For example, segment 1 extends from the top of the left hand side of the cut, in the counterclockwise direction, to the middle of the bottom of the cut (between the two asterisks). The numbers in the figure indicate the segments of the period 3 and period 2 orbits. Then a permutation matrix is defined which describes the forward time evolution of the system. This is a $(p_1 + p_2) \times (p_1 + p_2)$ matrix with the properties

$$P^{p_1 * p_2} = I_{p_1 + p_2}. \tag{13}$$

For example, forward time evolution causes the phase space point in the period-three orbit to evolve from segments $1 \rightarrow 2 \rightarrow 3 \rightarrow 1$. Thus, $P(1, 2) = P(2, 3) = P(3, 1) = 1$; similarly $P(4, 5) = P(5, 4) = 1$ for the period-two orbit (cf., Figure 9b). Finally, a crossing matrix C is defined. This describes which orbit segments cross over each other. This is a signed real symmetric $(p_1 + p_2) \times (p_1 + p_2)$ matrix with integer entries. This is constructed as follows. Segment 1 crosses in sequence segments 3 (+1) , 5 (+1), 2 (+1), 4 (+1), 4 (−1), and 2(−1). Then $C(1, 2) = +1 - 1 = 0$, $C(1, 3) = +1$, $C(1, 4) = +1 - 1 = 0$, and $C(1, 5) = +1$. The remaining elements in the crossing matrix are computed similarly. The crossing matrix for these two orbits is shown in Figure 9c.

During the first period, initial conditions at (i) and (j) will cross $C(i, j)$ number of times. During the second pass, they will cross $(P^{-1}CP)(i, j)$ times. Summing all crossings of initial conditions (i, j) for any i, j, we compute the matrix of relative rotation rates

$$2 \times p_1 \times p_2 \times RRR = \sum_{k=0}^{p_1 * p_2 - 1} \left((P^T)^k C P^k \right), \tag{14}$$

where $P^{-1} = P^T$ since P is a permutation matrix. The integer matrix $2 \times p_1 \times p_2 \times RRR$ is shown in Figure 9 for the orbits (011) and (01). From this matrix one easily determines the relative rotation rates for the period 2 and 3 orbits as well as the relative rotation rate of the period 2 orbit with itself and the period 3 orbit with itself.

There were no discrepancies between the relative rotation rates and self-relative rotation rates for all orbits extracted from the Belousov-Zhabotinskii data up to period 8 when computed from the reconstructed orbits or predicted from the template, with the exception of the period 4 (0111) and one of the period 7 (0101011) segments, as discussed above.

Table 4. Knot types of reconstructed periodic orbits.

Symbolics	Knot Type	Conway Polynomial	Remarks
1	trivial	$\nabla = 1$	
01	trivial	$\nabla = 1$	
011	trivial	$\nabla = 1$	
0111	torus $T_{2,3}$	$\nabla = 1 + z^2 \equiv \nabla_3$	first nontrivial
01011	torus $T_{2,5}$	$\nabla = 1 + 3z^2 + z^4 \equiv \nabla_5$	
0110M1	torus $T_{2,5}$	$\nabla = 1 + 3z^2 + z^4$	doubled from 011
0110101	pretzel $P_{7,3,-2}$	$\nabla = (1 + z^2)\nabla_9 + z^2\nabla_7$	first nontorus knot

$\nabla_7 = z^6 + 5z^4 + 6z^2 + 1$

$\nabla_9 = z^8 + 7z^6 + 15z^4 + 10z^2 + 1$

The knot polynomials were useful in the search for a period 6 orbit. Three orbital segments were identified in which the close return after six periods was closer than the return after three. In two instances in which the period 3 return map was fairly close, the symbolic dynamics was (011011). The knot polynomial indicated that the orbital segment followed the period 3 orbit closely for two full (period 3) periods. The third segment did not have a close return on the third period and had symbolic dynamics (0110M1), where M was the cut point (maximum) for symbolic dynamics in the return map. Its knot polynomial indicated it closely followed the period doubled orbit of the period 3, with symbolic dynamics (011001).

We computed the Conway polynomials for each of the periodic orbits listed in Table 1 up to period 7. These polynomials are presented in Table 4. The Conway polynomials for each of the knots reconstructed from the Belousov-Zhabotinskii data were computed using the standard rules [21]. Once again, the polynomials computed from the horseshoe template and those computed from the reconstructed orbits agreed in all instances [17].

7. Qualitative Dynamics

By identifying a template, we have provided a method to model the qualitative dynamics of the system. Once the template is known, so are some topological features of the orbits which can be extracted using the procedure described in Sec. 3. For example, we know that the extracted orbits can be arranged as positive braids, or that the (p, q) torus knots will have $p/q \leq 2/3$ [17]. But which of the orbits present in our induced template are actually present in the chaotic solution is an unsolved issue. The knowledge of how the orbits that are found are knotted in a "complicated" data set is not merely academic; the presence of certain kinds of orbits imply an entropy greater than zero (i.e., positive topological entropy). The reason is that some periodic behaviors imply, by continuity, a complicated behavior for the complement of the periodic orbit. The precise statement [22] is that in a flow there will be orbits that are neither rotations nor rotations around rotations if and only if the entropy is greater than zero. This remarkable result tells us that the mere existence of such an orbit is a sufficient condition for the "chaoticity" of the flow. In the horseshoe template there is

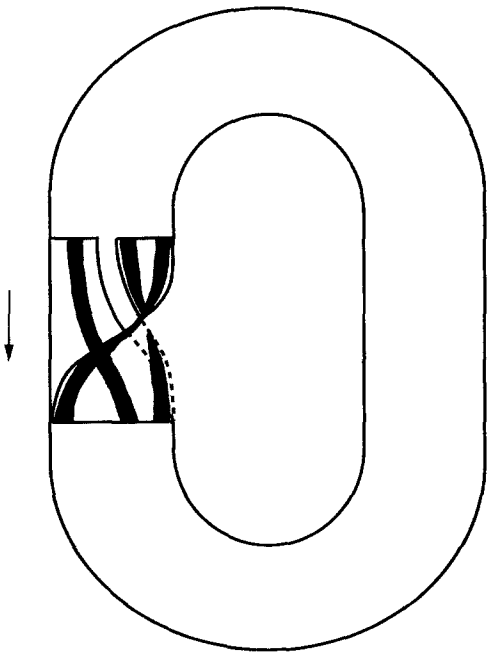

Fig. 10. The shaded region in the horseshoe template supports only torus knots. The flow is counterclockwise in this projection, from top to bottom in the two-branch region. All torus knots in this portion of the template consist of words composed of the letters 0 and 11 "as equally spaced as possible." All such torus knots are well-ordered. The presence of a period 7 "pretzel knot" P(7, 3, −2), which does not lie entirely within the shaded region, implies positive topological entropy.

definitely "space" for orbits that are neither rotations nor rotations around rotations, but it could be the case that embedded in our attractor there are only resonant torus knots (see Figure 10), their symbolic dynamics consisting of words built from letters 0 and 11 "as equally spaced as possible" (e.g., 011, 01101101111).

We have observed that the letter 0 is always followed by a 1 in this data set. The orbits (1), (01), (0111), (01110101) are rotations around rotations around . . . , the period doubling sequence. The period 5 orbit (01101) is the saddle node partner of (01111) and is therefore well ordered. The orbit (0110M1) is the double of the period 3 orbit. The lowest periodic orbit that is neither cabled nor well ordered and compatible with the observation above is the period 7 orbit (0101011). This orbit was reconstructed from the data. It was identified as a pretzel knot of type (7, 3, −2) [17]. An orbit knotted as a pretzel, not being a "hereditarily rotation compatible" (i.e., neither cabled nor well ordered) orbit [22], is a sufficient condition for stating that the entropy of the system is greater than zero.

8. Discussion

In the present work we have been concerned with establishing a practical procedure for analyzing and understanding chaotic time series data in a topological way. A number of questions have been raised in the course of the development and implementation of this topological method. These range from practical experimental questions to long-range theoretical issues. We have been able to address some of these questions, but not others. We feel it is important to state here those questions which remain unsolved.

A. Topological Questions

In the Birman-Williams theorem, periodic orbits embedded in a 3-manifold are projected along a contracting direction to a branched 2-manifold. All the knotting and linking information for the periodic orbits is preserved in the projection. If scalar time series from this three-dimensional flow are used to construct an induced template following the procedure described above, what is the relationship between the template for the original flow and the induced template for the embedded flow? Do embeddings using different variables (e.g., $y(t)$, or $z(t)$ instead of $x(t)$) induce identical templates?

We do not know the answer to these questions. For the Rossler attractor the original template and the three templates induced from $x(t)$, $y(t)$, and $z(t)$ are identical, up to handedness.

However, we point out that it may be possible to construct an induced template from a high-dimensional ($n > 3$) dynamical system for which the Birman-Williams theorem is not applicable. We do not know the conditions under which an induced template can be constructed from scalar data from an n-dimensional dynamical system, but we suspect that "strongly contracting" conditions can be found to extend the theorem to a class of flows in higher dimensions with only one unstable direction. A converse question can be posed. If a time series can be successfully embedded in three dimensions, does it mean that the flow can be described by a three-dimensional system of equations?

It is received wisdom that knots "fall apart" in $\mathbb{R}^n$, so that a topological description of periodic orbits in high-dimensional ($n > 3$) dynamical systems cannot be anticipated. While it is true that the linking of images of $S^1 \to \mathbb{R}^n$ ($n > 3$) cannot be defined, it is also true that periodic orbits in n-dimensional dynamical systems come "dressed" with stable and unstable invariant sets, and that (un)stable sets of distinct periodic orbits cannot intersect. As a result, it might be possible to define the linking of periodic orbits in $\mathbb{R}^n$ through the linking of their invariant sets. In fact, White [28] provides an elegant method for computing the linking number of manifolds M^m and K^k of dimension m and k in $\mathbb{R}^{m+k+1}$ in terms of a generalization of the Gaussian integral when the manifolds have no boundary. Thus, a key to extending topological analysis to n-dimensional systems is finding a way to associate manifolds without boundary to periodic orbits.

B. Close Returns

The first step in the topological analysis of data is the search for close returns. It is therefore important to explore the properties of this search.

This search can be carried out on scalar or vector data sets with and without first constructing an embedding. In this work we have carried out the search without embedding to show that the extraction of periodic orbits is independent of embedding. In general, embedding the data prior to the close returns search will clean up the close returns plot. For example, the data suggesting nonhorizontal line segments in Figure 2 are present because on the neighboring side of each minimum or maximum are data elements with nearly the same values. Such "accidental" close returns are not harmful to our search for long-lived close returns, represented by horizontal line segments, and are generically removed by almost any kind of embedding. The sharpened nature of the close returns search resulting from embedding can be seen in Figure 2 of [23].

The effect of noise on the search for close returns has been carried out and documented in [29]. The standard deviation, σ, for chaotic time series data generated by the Rossler attractor $(R(\sigma))$ was computed. An independent and identically distributed Gaussian random data set with mean 0 and standard deviation σ $(GIID(0, \sigma))$ was also generated. Then a data set $R(\sigma) + fGIID(0, \sigma)$ was generated by pointwise addition, $0 \leq f \leq 2$. The search for close returns was carried out on this mixture of chaotic and stochastic data. The close returns plot degraded very gracefully with additive noise, with close return line segments still clearly visible for $f \approx 0.4$. For $f = 2.0$ the close returns plot was not readily distinguishable from the close returns plot for a stochastic data set $(0.0R(\sigma) + 1.0 * GIID(0, \sigma))$. However, by noise averaging over 11 adjacent data values, it was possible to retrieve a clear return signal from the data set $R(\sigma) + fGIID(0, \sigma)$ with $f = 2.0$.

In these analyses the sample rate ranged from 50 to 150 measurements per characteristic period (i.e., returns to a Poincaré section) and data sets ranged from 20 to 500 periods.

A similar set of experiments was carried out on the Belousov-Zhabotinskii data. These data (64K) were sampled at about 120 samples per characteristic period and contained ~ 543 periods. The results differed in no substantial way from the analysis of the Rossler data set documented in [29].

C. Embedding

The entire question of embedding scalar data in $\mathbb{R}^3$ would benefit from more investigation. We have investigated several families of embeddings depending on parameters and found that the strange attractor can undergo self-intersections as the parameters are varied. We use embeddings which are optimized to display the topological properties of flows.

The phase space embedding which we prefer depends on successive differences. If such an embedding is possible, the coordinates satisfy equations of the form

$$\begin{aligned} \frac{dy_1}{dt} &= y_2, \\ \frac{dy_2}{dt} &= y_3, \\ \frac{dy_3}{dt} &= f(y_1, y_2, y_3). \end{aligned} \tag{15}$$

By plotting the phase portrait of this flow in the y_2, y_3 plane it is an easy matter to see that all periodic orbits must circle the y_1 axis, $y_2 = y_3 = 0$, in the same direction. Moreover, for every bounded periodic orbit, y_2 oscillates about 0 (see the first equation in 14); by the same token y_3 oscillates around 0; finally y_2 increases if $y_3 > 0$ and decreases if $y_3 < 0$ requiring the rotation of the orbit around the origin in the (y_2, y_3) plane. Thus, a half plane having the y_1 axis as boundary can serve as a control section. We call this plane a control section rather than a Poincaré section, since the flow might be tangent to the plane at some points.

Since it is almost always a bad idea to differentiate experimental data, differential phase space embeddings are not easy to construct. We could not construct such an embedding even on a very clean data set like the Belousov-Zhabotinskii data set which we used. Rather, we were driven to devise integral filters, so that the embedding still retained the important aspects of differential phase space embeddings.

D. Induced Templates

Under which conditions can we hope to induce a template from a chaotic data set? We cannot answer this question. Following our "de facto" approach we can say that in all the cases studied so far the association of a finite number of orbits with those on a template has been possible.

In constructing and verifying templates and induced templates we need to compute the linking numbers of pairs of low-period orbits. Inequivalent templates can give rise to the same spectra of periodic orbits and linking numbers. We know instances in which this occurs. The Borromean rings consist of a set of three rings mutually linked together although each pair is unlinked. It is possible to construct templates with three or more branches in which the period 1 orbits in each pair of branches have linking number zero, but the period 1 orbits in three or more branches cannot be unlinked. No two-point function (functions of pairs of orbits) can distinguish such a template from a template in which the three (or more) period 1 orbits in three or more branches are unlinked or even pairwise unlinked but linked in a different way. Such templates can only be distinguished by three-point functions, four-point functions, ... Fortunately, we have yet to encounter such complicated templates in physical systems or models of physical systems.

E. Template Verification

One expects the analysis of time series data to degrade as the noise level increases. In general, the lower the period of the orbit, the more robust it is against noise degradation. As the noise level increases, it is possible to extract a decreasing number of periodic orbits. The orbits which are lost are typically those of the highest period. Since the induced template construction depends only on the lowest-period orbits, it is very robust against noise. Verification of the induced template depends on orbits of higher period. Thus, as the noise level is increased, fewer orbits become available to verify the induced template. This in a sense is a reversal of Murphy's Law: as a general rule noise degrades the least important first and the most important last.

Verification of the template induced from the Belousov-Zhabotinskii data depended on proper identification of the orbits by their symbolic dynamics. This in turn was made relatively easy by the existence of an essentially one-dimensional return map. This raises two questions: Is a topological analysis useful when a symbolic dynamics is available? Under what conditions can we associate a symbolic name to an extracted periodic orbit?

To answer the first question, we note that two systems with identical return maps, and therefore identical symbolic dynamics, but differing in their global torsion, cannot be distinguished at the level of their mappings, but only at the topological level described here. This occurs, for example, for the Duffing equation [30]. Control parameter values in different "fingers" generate essentially identical return maps. However, the topological properties (global torsion) differ in a systematic way from one finger to another. Thus, the fingers in the control parameter space can be labeled by an integer n which identifies the global torsion of all orbits generated for those control parameter values as $2n + 1$.

The existence of a one-dimensional map in the case we studied is strictly related to a high degree of dissipation, but even in such a case we have to expect some violation of the symbolic dynamics generated by the map. By this we mean that the order associated with the kneading sequence will differ for some pair of points from the order in the interval and that the symbolic names of the orbits given by the one-dimensional map will differ from the (true and invariant) names deduced from the braid structure. This was seen explicitly for the period 6 orbit, identified through its knot polynomial, whose symbolic name (011001) is not compatible with the independent observation that in this data set passage through the orientation-preserving branch (0) is always followed by passage through the orientation-reversing branch (1) of the return map.

In the absence of a one-dimensional map, the process of giving symbolic names to the extracted orbits is "global", that is, it involves assigning names to all extracted orbits simultaneously. Usually several names are possible for each orbit. This procedure leads to a tedious but possible process of eliminating all those assignments incompatible with the braid structure. This procedure was successfully applied in previous work [9, 20, 30].

9. Summary and Conclusions

We were successful in constructing a three-dimensional embedding without self-intersections from the experimental data set. We were able to construct, for that flow, a template that is compatible with it, in the sense that every periodic orbit in the flow can be held by the proposed template. This template predicts the topological organization of all unstable periodic orbits buried in a strange attractor. The minimal information required to construct the template was extracted from the three lowest-period orbits.

In confronting experimental data we have encountered typical difficulties. All such difficulties have been overcome by perturbations of the general procedure described in Sec. 2.

The first step in template determination is reconstruction of periodic orbits from chaotic time series data. Such orbits are located by a search for close returns. This has

a particularly appealing graphical representation, as shown in Figure 2. This graphical representation is suggestive of a new class of tests for chaos which are topological yet quantitative at the same time.

The general theory of embeddings is in a preliminary stage of development. We have found a very nice embedding of the Belousov-Zhabotinskii data based on the introduction of filters. We suggest that the question of optimum filters for topological (as opposed to metric) properties is an area well worth pursuing.

Template determination proceeds algorithmically using the reconstructed and embedded period 1 and period 2 orbits. If some of these orbits are not available, the necessary information can be extracted from orbits of higher period. Not all orbits (0), (1), (01) are available from the Belousov-Zhabotinskii data; the template was reconstructed from the lowest-period orbits which were available: (1), (01), (011).

The correctness of the template identification can be checked by further computation. On the one hand, the template can be used to construct the linking and self-linking numbers of all orbits and orbit pairs, the local torsion of all orbits, the relative rotation rates of all orbits and orbit pairs, and, indirectly, the knot polynomials. On the other hand, all these quantities can be determined from the reconstructed orbits and their embeddings. A comparison between the predicted (from the template) and the measured (from the orbits) invariants can then be used to show that the template identification is incorrect, or else to provide additional confidence that it is correct.

The template serves to model the qualitative dynamics of the system generating the time series data.

Acknowledgments

We thank Prof. D. P. Lathrop for providing the Belousov-Zhabotinskii data file on which this work was based. We thank Prof. M. Valliéres for useful discussions, and F. Papoff for comparisons of data files from a laser with saturable absorber, which seems to be governed by a dynamics similar to that governing the Belousov-Zhabotinskii reaction. We also thank Prof. P. Holmes for providing useful comments and criticisms on an earlier version of this manuscript, and Profs. J. S. Birman and R. F. Williams for discussions about templates and their uses. One of the authors (R. G.) thanks another (M. A. N.) for the hospitality extended during a visit to Uppsala University. This work is partially supported by N.S.F. Grant PHY 88-43235.

References

1. G. B. Mindlin , X.-J. Hou, H. G. Solari, R. Gilmore, and N. B. Tufillaro, Classification of strange attractors by integers, Phys. Rev. Lett. **64**, 2350–2353 (1990).
2. K. Coffman, W. D. McCormick, Z. Noszticzius, R. H. Simoyi, and H. L. Swinney, Universality, multiplicity, and the effect of iron impurities in the Belousov-Zhabotinskii reaction, J. Chem. Phys. **86**, 119–129 (1987).
3. P. Richetti, P. De Keeper, J. C. Roux, and H. L. Swinney, A crisis in the Belousov-Zhabotinskii reaction: experiment and simulation, J. Stat. Phys. **48**, 977–990 (1987).
4. P. Grassberger and I. Procaccia, Estimation of the Kolmogorov entropy from a chaotic signal, Phys. Rev. A **28**, 2591–2593 (1983).

5. A. Wolf, J. B. Swift, H. L. Swinney, and J. A. Vastano, Determining Lyapunov exponents from a time series, Physica **16D**, 285–317 (1985).
6. C. Grebogi, E. Ott, and J. A. Yorke, Unstable periodic orbits and the dimension of chaotic attractors, Phys. Rev. A **36**, 3522–3524 (1987).
7. P. Cvitanovic, G. H. Gunaratne, and I. Procaccia, Topological and metric properties of Henon-type strange attractors, Phys. Rev. A **38**, 1503–1520 (1988).
8. G. H. Gunaratne, P. S. Linsay, and M. J. Vinson, Chaos beyond onset: a comparison of theory and experiment, Phys. Rev. Lett. **63**, 1–4 (1989).
9. N. B. Tufillaro, H. G. Solari, and R. Gilmore, Relative rotation rates: fingerprints for strange attractors, Phys. Rev. A **41**, 5717–5720 (1990).
10. T. C. Halsey, M. H. Jensen, L. P. Kadanoff, I. Procaccia, and B. I. Shraiman, Fractal measures and their singularities, Phys. Rev. A **33**, 1141–1151 (1986); **34**, 1601 (1986).
11. J. G. Caputo, Practical remarks on the estimation of dimension and entropy from experimental data, in *Measures of complexity and chaos* edited by N. B. Abraham, A. M. Albano, A. Passamante and P. Rapp, NATO Series B. **208**, 99–110 (1989).
12. R. Devaney and Z. Nitecki, Shift automorphisms and the Henon mapping, Commun. Math. Phys. **67**, 137–146 (1979).
13. J. S. Birman and R. F. Williams, Knotted periodic orbits in dynamical systems I: Lorenz's equations, Topology **22**, 47–82 (1983).
14. J. S. Birman and R. F. Williams, Knotted periodic orbits in dynamical systems II: knot holders for fibered knots, Cont. Math. **20**, 1–60 (1983).
15. P. Holmes, Knotted periodic orbits in suspensions of Smale's horseshoe: the period multiplying and cabled knots, Physica **21D**, 7–41 (1986).
16. P. Holmes, Knots and orbit geneaologies in nonlinear oscillators, in *New Directions in Dynamical Systems*, edited by T. Bedford and J. Swift, Cambridge U. Press., 1988, pp. 150–191.
17. P. Holmes and R. F. Williams, Knotted periodic orbits in suspensions of Smale's horseshoe: torus knots and bifurcation sequences, Arch. Rat. Mech. Anal. **90**, 115–194 (1985).
18. L. Gyorgyi, T. Turanyi, and R. J. Field, Mechanistic details of the oscillatory Belousov-Zhabotinskii reaction, J. Phys. Chem. **94**, 7162–7170 (1990).
19. T. Uezu and Y. Aizawa, Topological character of a periodic solution in three dimensional ordinary differential equation system, Prog. Theor. Phys. **68**, 1907–1916 (1982).
20. H. G. Solari and R. Gilmore, Relative rotation rates for driven dynamical systems, Phys. Rev. A **37**, 3096–3109 (1988).
21. L. H. Kauffman, *On Knots*, Princeton University Press, Princeton, New Jersey, 1987.
22. J. M. Gambaudo, S. Van Strien, and C. Tresser, The periodic orbit structure of orientation preserving diffeomorphisms on D^2 with topological entropy zero, Ann. Inst. Henri Poincaré **49**, 335–356 (1989).
23. D. P. Lathrop and E. J. Kostelich, Characterization of an experimental strange attractor by periodic orbits, Phys. Rev. A **40**, 4028–4031 (1989).
24. H. Whitney, Differentiable manifolds, Ann. Math. **37**, 645–680 (1936). *Geometric Integration Theory*, Princeton University Press, Princeton, New Jersey, 1957.
25. F. Takens, Detecting strange attractors in turbulence, Lecture Notes in Mathematics **898**, 366–381(1981).
26. A. M. Fraser, Information and entropy in strange attractors, IEEE Trans. Inf. Theory, **35**, 245–262 (1989).
27. R. Badii and A. Politi, Renyi dimensions from local expansion rates, Phys. Rev. **A35**, 1288-1293 (1988).
28. J. H. White, Self-linking and the Gauss integral in higher dimensions, Am. J. Math. **91**, 693–728 (1969).
29. C. Gilmore, A new test for chaos, J. Econ. Behavior and Organization, submitted.
30. H.G. Solari and R. Gilmore, Organization of periodic orbits in the driven Duffing oscillator, Phys. Rev. **A38**, 1566–1572 (1988).